Temporal variations of crustal structure in the source region of the 2007 Noto Hanto Earthquake, central Japan, with passive image interferometry

Shiro Ohmi[1], Kazuro Hirahara[2], Hiroo Wada[3], and Kiyoshi Ito[4]

[1]*Earthquake Hazards Division, Disaster Prevention Research Institute, Kyoto University, Gokasho, Uji 611-0011, Japan*
[2]*Graduate School of Science, Kyoto University, Kyoto 606-8502, Japan*
[3]*Kamitakara Observatory, Disaster Prevention Research Institute, Kyoto University, Takayama, Gifu 506-1317, Japan*
[4]*Research Center for Earthquake Prediction, Disaster Prevention Research Institute, Kyoto University, Gokasho, Uji 611-0011, Japan*

(Received July 14, 2007; Revised November 21, 2007; Accepted December 6, 2007; Online published November 7, 2008)

The passive image interferometry technique is applied to the continuous seismic waveform data obtained around the source region of the 2007 Noto Hanto Earthquake, central Japan. We computed the autocorrelation function (ACF) of band-pass filtered seismic noise portion recorded with each short-period seismometer at several seismic stations for 1 day each. In some stations, comparison of each 1-day ACF shows temporal evolutions of the ACF, which are interpreted as the change of seismic velocity structure in the volume considered. Sudden changes of ACF are detected to be associated with the occurrence of the main shock in one station of the four stations analyzed. Gradual changes of ACFs in the preceding 2 weeks of the main shock are also recognized in two stations, which would be of great importance for understanding the stress state before the occurrence of earthquakes.

Key words: Noto Hanto Earthquake, seismic interferometry, back ground noise, autocorrelation function.

1. Introduction

Recently, the 'seismic interferometry' technique has often been applied to retrieve the Earth's subsurface structure. The basic principle of the method is that the Green's function (seismic impulse response) between two seismometers can be retrieved by cross-correlation of a random isotropic wave field sensed at both instruments (e.g. Sanchez-Sesma and Campillo, 2006). Wapenaar (2004) revealed that body wave reflections from layer interfaces can be retrieved by cross-correlation as well as surface waves and turning waves. Green's function can be obtained from cross-correlation function (CCF) of diffusive part of multiple scattered seismic coda (Campillo and Paul, 2003) and also from the cross-correlation of ambient seismic noise (Shapiro and Campillo, 2004).

Retrieving Green's function from ambient noise is suited to the monitoring of temporal variations of the subsurface structure, because noise data are continuously available. Sens-Schönfelder and Wegler (2006) called this method 'passive image interferometry'. Although the CCF of the seismic noise portion recorded at two different receivers is usually used, Wegler and Sens-Schönfelder (2007) applied the autocorrelation function (ACF) of seismic noise recorded at a single station to retrieve the source-receiver collocated Green's function. Using the passive image interferometry technique, Wegler and Sens-Schönfelder (2007) revealed the temporal variation of the crustal structure in the vicinity of the source region of the 2004 Mid-Niigata earthquake, Japan. They detected that a sudden decrease of relative seismic velocity in the Earth's crust coincides with the occurrence of the earthquake, which is attributed to the decrease of stress caused by the mainshock.

On March 25, 2007, an M_w 6.6 earthquake occurred in the Noto Peninsula region, central Japan, which was named the 2007 Noto Hanto Earthquake by the Japan Meteorological Agency (JMA). The hypocenter of the earthquake determined by JMA is as follows: origin time = 09:41:57.9 JST on March 25, 2007; latitude = 37.220N; longitude = 136.685E; focal depth = 11 km (Fig. 1). In this paper, we present another application of the novel method of passive image interferometry to retrieve the temporal variation of the subsurface structure in the vicinity of the source region of the 2007 Noto Hanto Earthquake, central Japan.

2. Data and Method

We used vertical components of the continuous seismic noise data portion recorded at several short-period seismic stations around the source region of the 2007 Noto Hanto Earthquake. Figure 1 shows the distribution of the seismic stations used in this study together with the epicenter of the mainshock. The station N.TGIH is operated by NIED (National Research Institute for Earth Science and Disaster Prevention) and other three stations by DPRI (Disaster Prevention Research Institute) of Kyoto University.

We analyzed 6 months of data, about 4 months before and 2 months after the mainshock. The data were divided into 1-day (24 h) segments. The sampling frequency at each station is 100 Hz.

We first removed the DC offset of the data and applied appropriate band-pass filter to eliminate the effect of long-

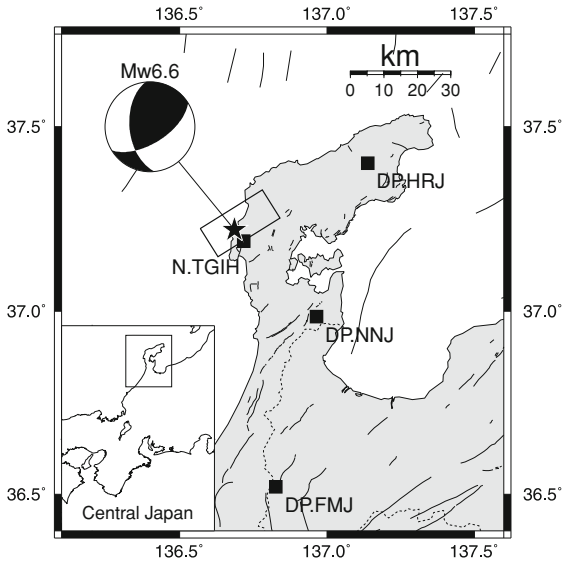

Fig. 1. Map around the epicenter of the 2007 Noto Hanto Earthquake, central Japan. Thick lines represent the active faults. Solid star denotes the epicenter of the mainshock, while solid squares represent seismic stations used in this study. Fault plane solution together with the surface projection of the fault plane obtained by Horikawa (2008) are also shown.

period tremor. We used the butterworth type band-pass filter of order eight (8). Pass band of the filter was selected to mark out the signal in ACF. Frequency bands of the filters applied to each station were as follows; 1.5 Hz–10 Hz for DP.HRJ and N.TGIH, and 2.0 Hz–10 Hz for DP.NNJ and DP.FMJ.

Next, in order to remove the effect of deterministic phases caused by earthquakes, we eliminated the earthquake signal portion from the records. First, we calculated the standard deviation of the amplitude of background noise portion with little earthquake signal. Based on the standard deviation of the noise amplitude, we determined an appropriate threshold value to detect the earthquake signal. Then we filled zero values into the seismic records where the amplitude is larger than the threshold. We tested several threshold values between 1 and 100 times the standard deviation. The test indicates that no significant differences in the pattern of ACFs are observed for threshold values smaller then 50, although relative amplitudes are changed. Thus, we used a threshold value of 10 times the standard deviation, as Wegler and Sens-Schönfelder (2007) used. Finally, we calculated the autocorrelation function (ACF) of the seismic record for 1 day. ACFs were calculated for each day during the target periods for all stations.

3. Temporal Variation of the Autocorrelation Functions

Figure 2(a)–(d) shows the temporal variation of ACFs for stations DP.NNJ (epicentral distance 36 km), DP.HRJ (45 km), N.TGIH (4 km), and DP.FMJ (79 km). Each plate consists of about 180 different ACFs, each of which was computed using the noise portion of 1 single day. In general, although the shape of ACF for each station is different to each other, the late phases in each station are quite coherent over ACFs of different days.

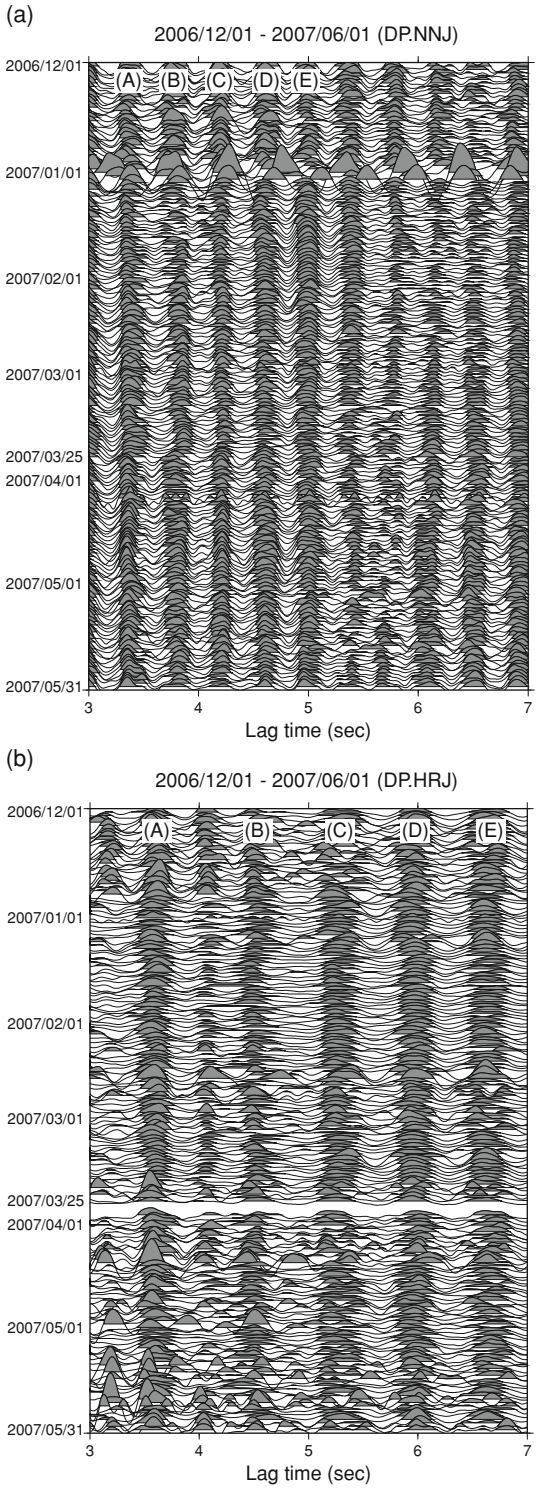

Fig. 2. Temporal variations of the ACF of seismic noise recorded at each station during 6 months. The ACF for a single day is shown as a function of the date. The 2007 Noto Hanto Earthquake occurred on March 25, 2007. Grey wiggles correspond to positive parts of the ACF. (a) ACF at station DP.NNJ (epicentral distance = 36 km). (b) ACF at station DP.HRJ (epicentral distance = 45 km). (c) ACF at station N.TGIH (epicentral distance = 4 km). (d) ACF at station DP.FMJ (epicentral distance = 79 km).

At DP.NNJ, late phases with a dominant frequency of about 2.5 Hz are seen. As we described in the previous section, we applied a band-pass filter before calculating ACFs, and it slightly affected the predominant frequency

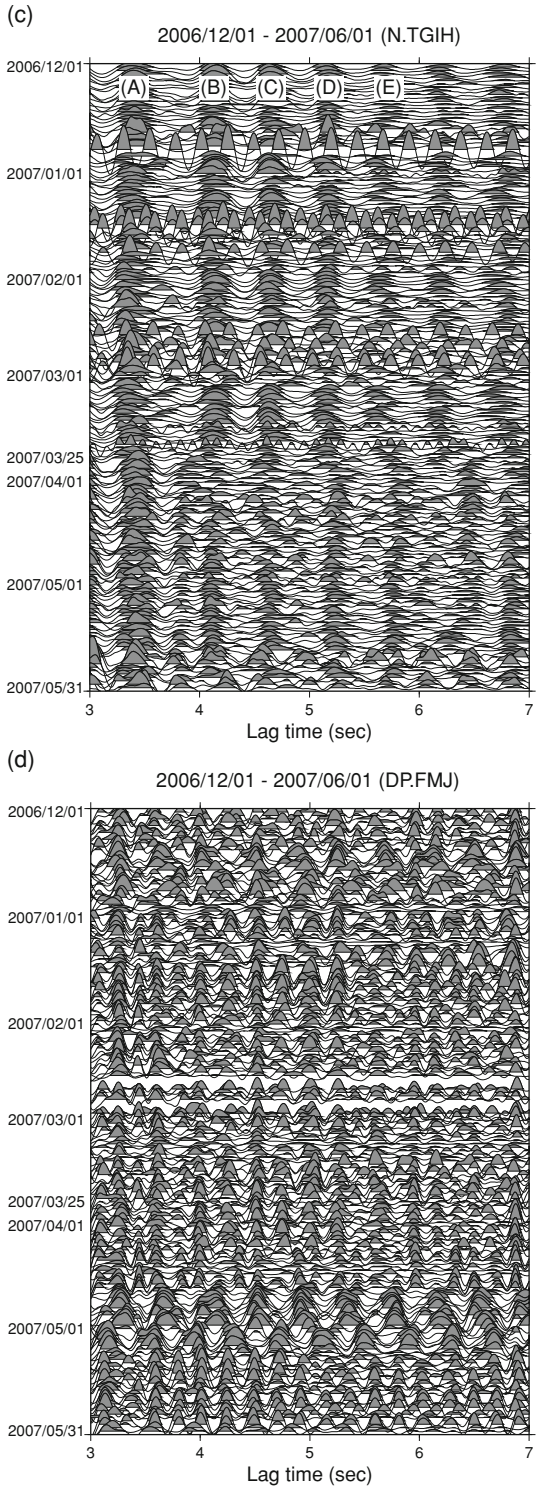

Fig. 2. (continued).

of the obtained ACFs. They are almost coherent over 6 months with little temporal variations (Fig. 2(a)). Changes in the lag time of the ACF are recognized in some parts. Figure 3(a) and (b) shows the relative time shifts of several clear phases shown in Fig. 2(a). To obtain the relative time shifts, we first stacked all the ACFs over 6 months to make 'master ACF' and then calculated the relative time shifts of five phases in Fig. 2(a) together with the correlation coefficients of the shape of the phases to those of 'master ACF'. Time ranges of selected phases A, B, C, D, and E are 3.14 s–3.58 s, 3.58 s–4.00 s, 4.00 s–4.40 s, 4.40 s–4.81 s, and 4.81 s–5.27 s, respectively. Time shifts of the phases whose correlation coefficients larger than 0.75 are shown. Phases A, B, and C exhibited gradual increases of the lag time within 2 weeks preceding the earthquake and they recovered just before or with the occurrence of the mainshock. Maximum time shift of about 0.05 s is observed on the phase B.

At DP.HRJ, where the predominant frequency of ACF is around 1.3 Hz, several clear phases are also seen (Fig. 2(b)). We again selected five phases to calculate relative time shifts. Time ranges of selected phases A, B, C, D, and E are 3.32 s–3.84 s, 4.31 s–4.77 s, 5.00 s–5.66 s, 5.66 s–6.34 s, and 6.34 s–7.00 s, respectively (Fig. 3(c) and (d)). Slight changes in lag time are observed in phases C, D, and E around the occurrence of the mainshock, though, the shapes of the ACFs are less stable with time compared to those at station DP.NNJ. Phases C, D, and E exhibit a gradual decrease of lag time within 2 weeks preceding the earthquake. Just before or with the occurrence of the mainshock, lag times of phases D and E recovered to the previous values, while phase C became rather unstable.

At station N.TGIH, which is the closest to the source area with the epicentral distance of 4 km, increase of the lag time of several phases are observed after the mainshock (Fig. 2(c)). We selected five phases to calculate relative time shifts (Fig. 3(e)). Time ranges of selected phases A, B, C, D, and E are 3.18 s–3.66 s, 3.93 s–4.40 s, 4.40 s–4.82 s, 4.82 s–5.44 s, and 5.44 s–6.00 s, respectively. Although severe turbulence in the shape of ACF during several days after the mainshock are seen in phases B, C, D, and E, a clear increase of the lag time is observed on these phases. It is also seen that the time shift is the smallest on phase A and the largest on phase E.

At DP.FMJ, whose epicentral distance is about 79 km, although several phases are observed, it is difficult to identify these phases over the period analyzed (Fig. 2(d)).

4. Discussion

Observed features of the ACFs are summarized as follows. At DP.NNJ, several clear phases exhibit a gradual increase of the lag time within 2 weeks preceding the mainshock and they recovered just before or with the occurrence of the mainshock (Fig. 3(a) and (b)). At DP.HRJ, on the contrary, several phases exhibit a gradual decrease of the lag time within 2 weeks preceding the mainshock, that recovered just before or with the occurrence of the mainshock (Fig. 3(c) and (d)). At N.TGIH, in spite of severe turbulence during several days after the mainshock, a clear increase of lag time is observed in several phases (Fig. 3(e)). At DP.FMJ, it is difficult to identify particular phases over the 6 months analyzed.

Except for some unexplainable turbulence (e.g. ACFs on the beginning of January 2007 at station DP.NNJ in Fig. 2(a)), most of the phases in ACFs are traceable with time. Focusing on these relatively stable ACFs, there are two remarkable features in the observed ACFs, as described in the previous section. One is that phases with a predominant frequency in ACF at one station are coherent over dif-

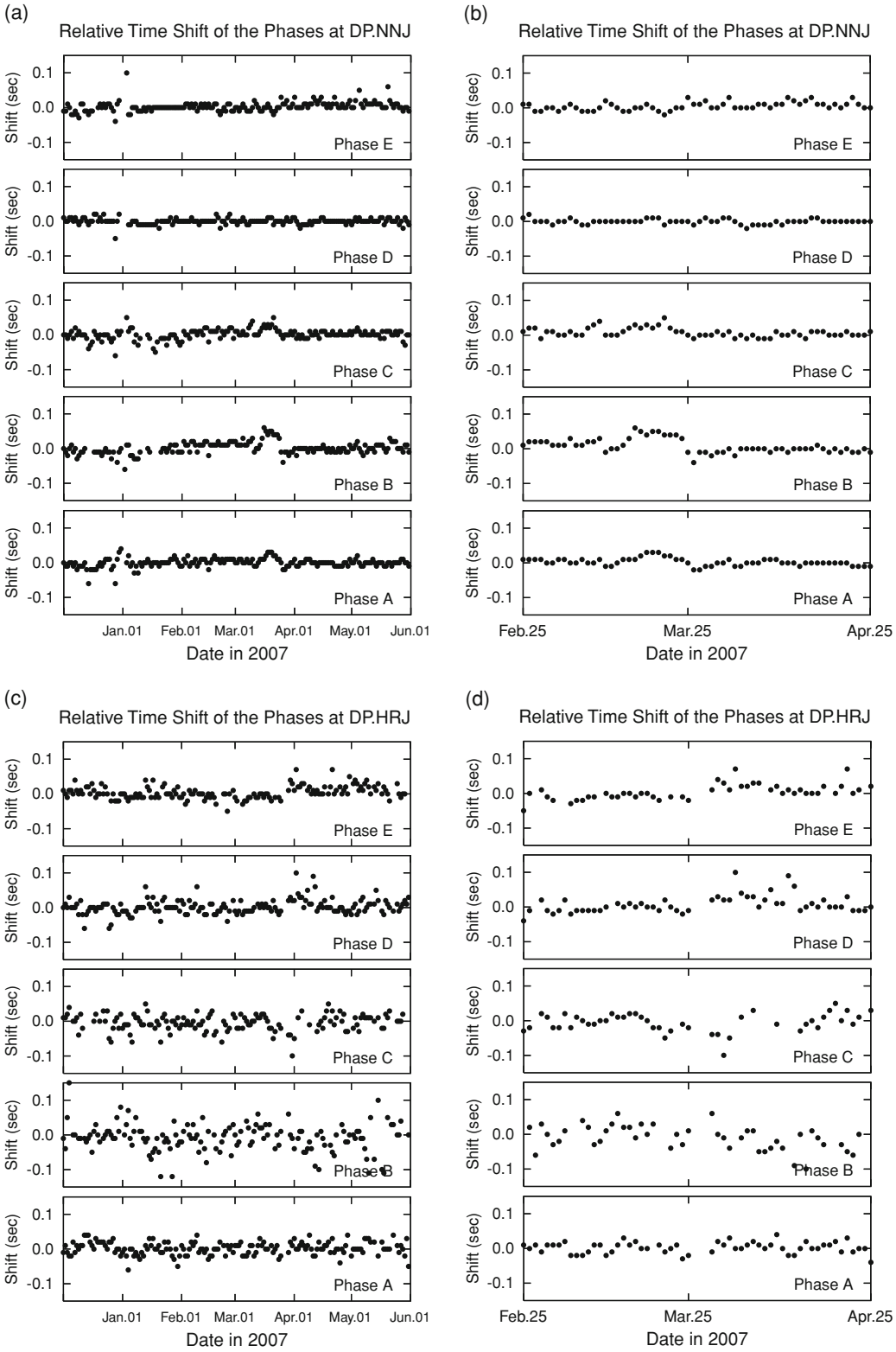

Fig. 3. Relative time shifts of several particular phases at each station. Time shifts are calculated by taking cross-correlation among the focused phases in ACFs. Only time shifts of the phases whose correlation coefficients larger than 0.75 are plotted. (a) Relative time shifts at station DP.NNJ during a period of 6 months. (b) Same as (a) but for during the period of 2 months including the occurrence of the earthquake for enlarged time window. (c) Relative time shifts at station DP.HRJ during 6 months. (d) Same as (c) but for during 2 months for enlarged time window. (e) Relative time shifts at station N.TGIH during 6 months.

ferent days, though the shape of ACF at each station is different to each other. In other words, the shapes of ACFs are temporally stable. The other is that the temporal evolutions of particular phases in ACF are sometimes observed around the occurrence of the earthquake. In other words, the lag times of particular phases are temporally changed before or after the earthquake.

Temporal stability of the ACF suggests the potentiality

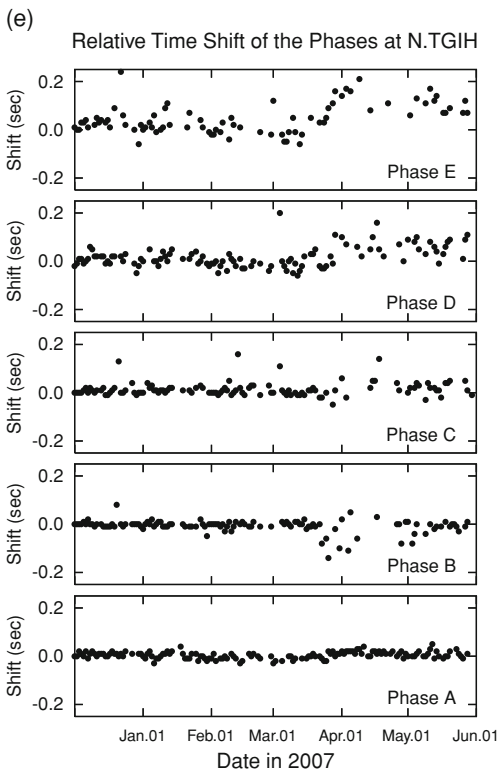

Fig. 3. (continued).

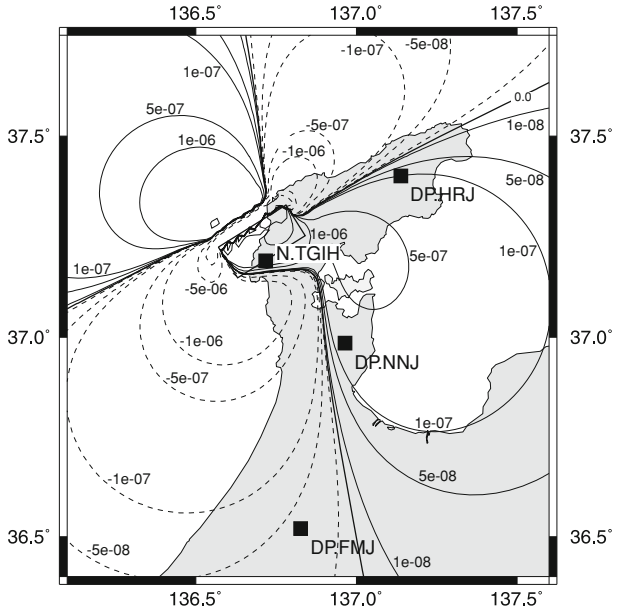

Fig. 4. Change in volumetric strain caused by the mainshock. Fault parameters obtained by Horikawa (2008) are assumed. Open rectangle shows the surface projection of the fault plane model. Solid line contours denote dilatation while dashed line contours show contraction.

for estimating the deep structure beneath the station. ACF of the background noise is proven to be a pseudo seismic reflection profile of the observation site, and therefore, if the shape of ACF is temporally stable, seismic reflection profile of deep portion can be obtained by stacking ACFs.

Change in the lag time of particular phases in ACFs is primarily attributed to the change of seismic wave velocity structure beneath the observation site. In general, the increase in the lag time of phases in ACF is caused by decreases of seismic wave velocity, and vice versa. Changes in wave velocity will be caused by several factors. Some candidates are as follows; (1) change in stress in the Earth's interior caused by the earthquake (e.g. Nishimura *et al.*, 2000; Poupinet *et al.*, 1984); (2) change in the near-surface material properties, such as generation of damage or cracks caused by the strong shaking of the earthquake (e.g. Peng and Ben-Zion, 2006); (3) change of degree of water saturation in the near-surface (e.g. Sens-Schönfelder and Wegler, 2006).

Figure 4 shows the change in volumetric strain caused by the mainshock. We assume the fault model obtained by Horikawa (2008), whose surface projection is shown by a rectangle in Fig. 4. The fault length, width, strike, dip, rake, and average slip are 22 km, 20 km, 58 deg, 60 deg, 135 deg, and 76.7 cm, respectively. Based on Okada (1992), we calculate the strain field. Stations DP.NNJ, DP.HRJ, and N.TGIH are located in the area of dilatation, while DP.FMJ is located in the area of contraction. In the area of dilatation, it is expected that there will be an increase in lag time of phases (positive time shift) in ACF due to a decrease of seismic velocity (e.g. Nishimura *et al.*, 2000). The ACF at station N.TGIH, closest to the source area, is the only one showing an increase in lag time after the earthquake. Thus, one possible cause of the time shift at N.TGIH may be the change in the stress field due to the earthquake. On the other hand, ACFs at stations DP.NNJ and DP.HRJ do not show such positive time shifts after the earthquake. DP.FMJ is located in the area of contraction. However, since it is difficult to trace particular phases over the period analyzed at this station, it is hard to recognize the change of time shifts with the occurrence of the mainshock.

At N.TGIH, another possible interpretation of the clear increase of lag time can be proposed. As we mentioned in the previous section, the time shift is the smallest on the phase of the shortest lag time, and the largest time shift is observed on the phase of the longest lag time. This result is likely attributed to the reverberation of the seismic wave in a shallow layer, in which seismic wave velocity decreased. Multiple reflection in the shallow layer causes the elongation of the time shift of each phase. Decrease of seismic wave velocity is probably caused by the change in the near-surface material properties by the strong shaking. Since we observed only ACF (autocorrelation function) at a single station, it is difficult to distinguish whether the signal has its origin in the deeper portion or just in the surface layer. Deploying a small-sized seismic array to compare autocorrelation function (ACF) and cross-correlation function (CCF) of the observation sites will provide useful information to delineate the origin of the phases as well as the subsurface structure (e.g. Draganov *et al.*, 2007).

At DP.NNJ and DP.HRJ, temporal evolution of ACF preceding the mainshock is detected. Although it is difficult to give a concrete interpretation of the observed features at present, a reliable interpretation would be of great importance for understanding the stress state before occurrence of earthquakes. It is also essentially important to conduct correlation analysis of other geophysical observations.

5. Conclusion

Temporal variation of the autocorrelation function (ACF) of ambient seismic noise around the source region of the 2007 Noto Hanto Earthquake is preliminarily analyzed to detect any possible change in the subsurface structure associated with the earthquake. Sudden change in lag time of the ACF associated with the occurrence of the mainshock is detected in some stations.

Station N.TGIH, with the epicentral distance of 4 km, showed an increase in lag time of the ACF, which is primarily attributed to the decrease of seismic wave velocity in the volume considered. Two possible interpretations are proposed. One is that the decrease of stress induced by the mainshock caused seismic wave velocity decreased. The other is that strong shaking produced a change in the near-surface material properties that caused the seismic wave velocity decreased.

At DP.NNJ and DP.HRJ, several clear phases in ACF exhibit gradual time shifts within 2 weeks preceding the mainshock and they recovered before or with the occurrence of the mainshock. Positive time shifts (increase of lag time) were observed at DP.NNJ, while negative time shifts (decrease of lag time) were recognized at DP.HRJ. Although it is difficult to give concrete interpretation of the observed features at DP.NNJ and DP.HRJ at present, it would be of great importance for understanding the stress state before the earthquake.

Acknowledgments. Seismic wave form data at Hi-net station N.TGIH is used in the study. Two anonymous reviewers provided critical comments that improved the manuscript. We are grateful to Dr. Takashi Iidaka for his continuous encouragement. The Generic Mapping Tools (Wessel and Smith, 1998) was used for drawing figures.

References

Campillo, M. and A. Paul, Long-range correlations in the diffuse seismic coda, *Science*, **299**, 547–549, doi:10.1126/science.1078551, 2003.

Draganov, D., K. Wapenaar, W. Mulder, J. Singer, and A. Verdel, Retrieval of reflections from seismic background-noise measurements, *Geophys. Res. Lett.*, **34**, L04305, doi:10.1029/2006GL028735, 2007.

Horikawa, H., Characterization of the 2007 Noto Hanto, Japan, earthquake, *Earth Planets Space*, **60**, this issue, 1017–1022, 2008.

Nishimura, T., N. Uchida, H. Sato, M. Ohtake, S. Tanaka, and H. Hamaguchi, Temporal changes of the crustal structure associated with the M6.1 earthquake on September 3, 1998 and the volcanic activity of mount Iwate, Japan, *Geophys. Res. Lett.*, **27**(2), 269–272, 2000.

Okada, Y., Internal deformation due to shear and tensile faults in a half-space, *Bull. Seismol. Soc. Am.*, **82**, 1018–1040, 1992.

Peng, Z. and Y. Ben-Zion, Temporal changes of shallow seismic velocity around the Karaderc-Duzce branch of the north Anatolian fault and strong ground motion, *Pure Appl. Geophys.*, **163**, 567–600, 2006.

Poupinet, G., W. L. Ellsworth, and J. Frechet, Monitoring velocity variations in the crust using earthquake doublets: an application to the Calaveras fault, California, *J. Geophys. Res.*, **89**, 5719–5731, 1984.

Sanchez-Sesma, F. J. and M. Campillo, Retrieval of the Green function from cross-correlation: The canonical elastic problem, *Bull. Seismol. Soc. Am.*, **96**, 1182–1191, 2006.

Sens-Schönfelder, C. and U. Wegler, Passive image interferometry and seasonal variations of seismic velocities at Merapi Volcano, Indonesia, *Geophys. Res. Lett.*, **33**, L21302, doi:10.1029/2006GL027797, 2006.

Shapiro, N. M. and M. Campillo, Emergence of broadband Rayleigh waves from correlations of the ambient seismic noise, *Geophys. Res. Lett.*, **31**, L07614, doi:10.1029/2004GL019491, 2004.

Wapenaar, K., Retrieving the elastdynamic Green's function of an arbitrary inhomogeneous medium by cross correlation, *Phys. Rev. Lett.*, **93**(254301), 1–4, 2004.

Wegler, U. and C. Sens-Schönfelder, Fault zone monitoring with passive image interferometry, *Geophys. J. Int.*, **168**, 1029–1033, 2007.

Wessel, P. and W. H. F. Smith, New, improved version of the Generic Mapping Tools released, *EOS, Trans. Am. Geophys. Union, Washington, D.C.*, **79**, 579, 1998.

S. Ohmi (e-mail: ohmi@eqh.dpri.kyoto-u.ac.jp), K. Hirahara, H. Wada, and K. Ito